

Characterizing a benchmark scenario for heavy Higgs boson searches in the Georgi-Machacek model

Heather E. Logan* and Mark B. Reimer

*Ottawa-Carleton Institute for Physics, Carleton University,
1125 Colonel By Drive, Ottawa, Ontario K1S 5B6, Canada*

(Dated: September 6, 2017)

The Georgi-Machacek model is used to motivate and interpret LHC searches for doubly- and singly-charged Higgs bosons decaying into vector boson pairs. In this paper we study the constraints on and phenomenology of the “H5plane” benchmark scenario in the Georgi-Machacek model, which has been proposed for use in these searches. We show that the entire H5plane benchmark is compatible with the LHC measurements of the 125 GeV Higgs boson couplings. We also point out that, over much of the H5plane benchmark, the lineshapes of the two CP-even neutral heavy Higgs bosons H and H_5^0 will overlap and interfere when produced in vector boson fusion with decays to W^+W^- or ZZ . Finally we compute the decay branching ratios of the additional heavy Higgs bosons within the H5plane benchmark to facilitate the development of search strategies for these additional particles.

* logan@physics.carleton.ca

I. INTRODUCTION

Since the discovery of a Standard Model (SM)-like Higgs boson at the CERN Large Hadron Collider (LHC) in 2012 [1], much experimental and theoretical attention has been devoted to testing the possibility that the Higgs sector contains additional scalars beyond the single SM isospin doublet. An interesting possibility among these extensions is that part of electroweak symmetry breaking—and hence part of the masses of the W and Z bosons—could be generated by scalars in isospin representations larger than the doublet. A prototype model in this class is the Georgi-Machacek (GM) model [2, 3], which contains a real and a complex isospin-triplet scalar in addition to the usual SM Higgs doublet.

A key feature of the GM model is the presence of doubly- and singly-charged Higgs bosons, $H_5^{\pm\pm}$ and H_5^\pm , that couple to SM vector boson pairs with an interaction strength proportional to the vacuum expectation value (vev) of the triplets. Constraining this coupling therefore directly constrains the allowed contribution of the triplets to the masses of the W and Z bosons. LHC searches for these scalars have been performed with production via vector boson fusion and decays to a pair of vector bosons [4–6]; the LHC measurement of the like-sign W boson cross section in vector boson fusion [7] also provides sensitivity to the doubly-charged scalar [8]. When the branching ratios of $H_5^{\pm\pm}$ and H_5^\pm to vector boson pairs are essentially 100%, these searches directly constrain the triplet vev v_χ as a function of the common mass m_5 of these scalars.

To aid the interpretation of these and future similar searches, the LHC Higgs Cross Section Working Group recently developed the “H5plane” benchmark scenario for the GM model [9]. The H5plane benchmark depends on two free input parameters, m_5 and $s_H \equiv \sqrt{8}v_\chi/v$ (where $v = (\sqrt{2}G_F)^{-1/2}$ is the SM Higgs vev), and the production cross sections for $H_5^{\pm\pm}$ and H_5^\pm in vector boson fusion are proportional to s_H^2 . The other parameters of the model are fixed in the benchmark so that $\text{BR}(H_5 \rightarrow VV) = 1$ to a very good approximation. Predictions for the production cross sections (at next-to-next-to-leading order in QCD) and decay widths of these scalars have been provided in the context of the H5plane benchmark for LHC collisions at 8 [10] and 13 TeV [9].

In this paper we perform the first comprehensive survey of the phenomenology of the H5plane benchmark in the GM model. We show that the entire H5plane benchmark is compatible with the LHC measurements of the 125 GeV Higgs boson couplings from 7 and 8 TeV data [11]. We point out that, over much of the H5plane benchmark, the lineshapes of the two CP-even neutral heavy Higgs bosons H and H_5^0 will overlap and interfere when these scalars are produced in vector boson fusion with decays to W^+W^- or ZZ . We also display the decay branching ratios of the additional heavy Higgs bosons within the H5plane benchmark to facilitate the development of search strategies for these additional particles. Our numerical work is done using the public code **GMCALC 1.2.1** [12].

This paper is organized as follows. In the next section we review the GM model and the specification of the H5plane benchmark. Section III contains the bulk of our results. We conclude in Sec. IV.

II. GEORGI-MACHACEK MODEL

The scalar sector of the GM model [2, 3] consists of the usual complex doublet $(\phi^+, \phi^0)^T$ with hypercharge¹ $Y = 1$, a real triplet $(\xi^+, \xi^0, -\xi^{++})^T$ with $Y = 0$, and a complex triplet $(\chi^{++}, \chi^+, \chi^0)^T$ with $Y = 2$. The doublet is responsible for the fermion masses as in the SM. Custodial symmetry, required in order to avoid stringent constraints from the ρ parameter, is preserved at tree level by imposing a global $\text{SU}(2)_L \times \text{SU}(2)_R$ symmetry on the scalar potential. To make this symmetry explicit, we write the doublet in the form of a bidoublet Φ and combine the triplets into a bitriplet X :

$$\Phi = \begin{pmatrix} \phi^{0*} & \phi^+ \\ -\phi^{++*} & \phi^0 \end{pmatrix}, \quad X = \begin{pmatrix} \chi^{0*} & \xi^+ & \chi^{++} \\ -\chi^{++*} & \xi^0 & \chi^+ \\ \chi^{++*} & -\xi^{++*} & \chi^0 \end{pmatrix}. \quad (1)$$

The vevs are given by $\langle \Phi \rangle = \frac{v_\phi}{\sqrt{2}} I_{2 \times 2}$ and $\langle X \rangle = v_\chi I_{3 \times 3}$, where $I_{n \times n}$ is the $n \times n$ unit matrix and the W and Z boson masses constrain

$$v_\phi^2 + 8v_\chi^2 \equiv v^2 = \frac{1}{\sqrt{2}G_F} \approx (246 \text{ GeV})^2. \quad (2)$$

¹ We use $Q = T^3 + Y/2$.

The most general gauge-invariant scalar potential involving these fields that conserves custodial SU(2) is given, in the conventions of Ref. [13], by²

$$\begin{aligned} V(\Phi, X) = & \frac{\mu_2^2}{2} \text{Tr}(\Phi^\dagger \Phi) + \frac{\mu_3^2}{2} \text{Tr}(X^\dagger X) + \lambda_1 [\text{Tr}(\Phi^\dagger \Phi)]^2 + \lambda_2 \text{Tr}(\Phi^\dagger \Phi) \text{Tr}(X^\dagger X) \\ & + \lambda_3 \text{Tr}(X^\dagger X X^\dagger X) + \lambda_4 [\text{Tr}(X^\dagger X)]^2 - \lambda_5 \text{Tr}(\Phi^\dagger \tau^a \Phi \tau^b) \text{Tr}(X^\dagger t^a X t^b) \\ & - M_1 \text{Tr}(\Phi^\dagger \tau^a \Phi \tau^b) (U X U^\dagger)_{ab} - M_2 \text{Tr}(X^\dagger t^a X t^b) (U X U^\dagger)_{ab}. \end{aligned} \quad (3)$$

Here the SU(2) generators for the doublet representation are $\tau^a = \sigma^a/2$ with σ^a being the Pauli matrices, the generators for the triplet representation are

$$t^1 = \frac{1}{\sqrt{2}} \begin{pmatrix} 0 & 1 & 0 \\ 1 & 0 & 1 \\ 0 & 1 & 0 \end{pmatrix}, \quad t^2 = \frac{1}{\sqrt{2}} \begin{pmatrix} 0 & -i & 0 \\ i & 0 & -i \\ 0 & i & 0 \end{pmatrix}, \quad t^3 = \begin{pmatrix} 1 & 0 & 0 \\ 0 & 0 & 0 \\ 0 & 0 & -1 \end{pmatrix}, \quad (4)$$

and the matrix U , which rotates X into the Cartesian basis, is given by [14]

$$U = \begin{pmatrix} -\frac{1}{\sqrt{2}} & 0 & \frac{1}{\sqrt{2}} \\ -\frac{i}{\sqrt{2}} & 0 & -\frac{i}{\sqrt{2}} \\ 0 & 1 & 0 \end{pmatrix}. \quad (5)$$

The physical fields can be organized by their transformation properties under the custodial SU(2) symmetry into a fiveplet, a triplet, and two singlets. The fiveplet and triplet states are given by

$$\begin{aligned} H_5^{++} &= \chi^{++}, & H_5^+ &= \frac{(\chi^+ - \xi^+)}{\sqrt{2}}, & H_5^0 &= \sqrt{\frac{2}{3}} \xi^{0,r} - \sqrt{\frac{1}{3}} \chi^{0,r}, \\ H_3^+ &= -s_H \phi^+ + c_H \frac{(\chi^+ + \xi^+)}{\sqrt{2}}, & H_3^0 &= -s_H \phi^{0,i} + c_H \chi^{0,i}, \end{aligned} \quad (6)$$

where the vevs are parameterized by

$$c_H \equiv \cos \theta_H = \frac{v_\phi}{v}, \quad s_H \equiv \sin \theta_H = \frac{2\sqrt{2}v_\chi}{v}, \quad (7)$$

and we have decomposed the neutral fields into real and imaginary parts according to

$$\phi^0 \rightarrow \frac{v_\phi}{\sqrt{2}} + \frac{\phi^{0,r} + i\phi^{0,i}}{\sqrt{2}}, \quad \chi^0 \rightarrow v_\chi + \frac{\chi^{0,r} + i\chi^{0,i}}{\sqrt{2}}, \quad \xi^0 \rightarrow v_\chi + \xi^{0,r}. \quad (8)$$

The masses within each custodial multiplet are degenerate at tree level and can be written (after eliminating μ_2^2 and μ_3^2 in favor of the vevs) as³

$$\begin{aligned} m_5^2 &= \frac{M_1}{4v_\chi} v_\phi^2 + 12M_2 v_\chi + \frac{3}{2} \lambda_5 v_\phi^2 + 8\lambda_3 v_\chi^2, \\ m_3^2 &= \frac{M_1}{4v_\chi} (v_\phi^2 + 8v_\chi^2) + \frac{\lambda_5}{2} (v_\phi^2 + 8v_\chi^2) = \left(\frac{M_1}{4v_\chi} + \frac{\lambda_5}{2} \right) v^2. \end{aligned} \quad (10)$$

The two custodial-singlet mass eigenstates are given by

$$h = \cos \alpha \phi^{0,r} - \sin \alpha H_1^{0\prime}, \quad H = \sin \alpha \phi^{0,r} + \cos \alpha H_1^{0\prime}, \quad (11)$$

where

$$H_1^{0\prime} = \sqrt{\frac{1}{3}} \xi^{0,r} + \sqrt{\frac{2}{3}} \chi^{0,r}, \quad (12)$$

² A translation table to other parameterizations in the literature has been given in the appendix of Ref. [13].

³ Note that the ratio M_1/v_χ can be written using the minimization condition $\partial V/\partial v_\chi = 0$ as

$$\frac{M_1}{v_\chi} = \frac{4}{v_\phi^2} \left[\mu_3^2 + (2\lambda_2 - \lambda_5)v_\phi^2 + 4(\lambda_3 + 3\lambda_4)v_\chi^2 - 6M_2 v_\chi \right], \quad (9)$$

which is finite in the limit $v_\chi \rightarrow 0$.

Fixed parameters	Variable parameters	Dependent parameters
$G_F = 1.1663787 \times 10^{-5} \text{ GeV}^{-2}$	$m_5 \in [200, 3000] \text{ GeV}$	$\lambda_2 = 0.4(m_5/1000 \text{ GeV})$
$m_h = 125 \text{ GeV}$	$s_H \in (0, 1)$	$M_1 = \sqrt{2}s_H(m_5^2 + v^2)/v$
$\lambda_3 = -0.1$		$M_2 = M_1/6$
$\lambda_4 = 0.2$		

TABLE I. Specification of the H5plane benchmark scenario for the Georgi-Machacek model. These input parameters correspond to `INPUTSET = 4` in `GMCALC` [12].

and we will use the shorthand $c_\alpha \equiv \cos \alpha$, $s_\alpha \equiv \sin \alpha$. The mixing angle α and masses are given by

$$\begin{aligned} \sin 2\alpha &= \frac{2\mathcal{M}_{12}^2}{m_H^2 - m_h^2}, & \cos 2\alpha &= \frac{\mathcal{M}_{22}^2 - \mathcal{M}_{11}^2}{m_H^2 - m_h^2}, \\ m_{h,H}^2 &= \frac{1}{2} \left[\mathcal{M}_{11}^2 + \mathcal{M}_{22}^2 \mp \sqrt{(\mathcal{M}_{11}^2 - \mathcal{M}_{22}^2)^2 + 4(\mathcal{M}_{12}^2)^2} \right], \end{aligned} \quad (13)$$

where we choose $m_h < m_H$, and

$$\begin{aligned} \mathcal{M}_{11}^2 &= 8\lambda_1 v_\phi^2, \\ \mathcal{M}_{12}^2 &= \frac{\sqrt{3}}{2} v_\phi [-M_1 + 4(2\lambda_2 - \lambda_5) v_\chi], \\ \mathcal{M}_{22}^2 &= \frac{M_1 v_\phi^2}{4v_\chi} - 6M_2 v_\chi + 8(\lambda_3 + 3\lambda_4) v_\chi^2. \end{aligned} \quad (14)$$

A. H5plane benchmark

The H5plane benchmark scenario for the GM model was introduced in Ref. [9]. It is designed to facilitate LHC searches for $H_5^{\pm\pm}$ and H_5^\pm in vector boson fusion with decays to $W^\pm W^\pm$ and $W^\pm Z$, respectively. It is specified as in Table I, in a form that is easily implemented in the model calculator `GMCALC` [12]. After imposing the existing direct search constraints on $H_5^{\pm\pm}$, the benchmark has the following features:

- It comes close to fully populating the theoretically-allowed region of the $m_5 - s_H$ plane for $m_5 \in [200, 3000] \text{ GeV}$, as shown in Fig. 1 (see below).
- It has $m_3 > m_5$ over the whole benchmark plane, so that the Higgs-to-Higgs decays $H_5 \rightarrow H_3 H_3$ and $H_5 \rightarrow H_3 V$ are kinematically forbidden, leaving only the decays $H_5 \rightarrow VV$ at tree level; i.e., $\text{BR}(H_5 \rightarrow VV) = 1$.
- The entire benchmark satisfies indirect constraints from B physics, the most stringent of which is $b \rightarrow s\gamma$ [15].
- The region still allowed by direct searches is currently unconstrained by LHC measurements of the couplings of the 125 GeV Higgs boson, as we will show in this paper.

In `INPUTSET = 4` of `GMCALC`, the nine parameters of the scalar potential in Eq. (3) are fixed in terms of the nine input parameters m_h , m_5 , s_H , λ_2 , λ_3 , λ_4 , M_1 , M_2 , and $v = (\sqrt{2}G_F)^{-1/2}$. The quartic coupling λ_5 is computed from these using

$$\lambda_5 = \frac{2m_5^2}{3c_H^2 v^2} - \frac{\sqrt{2}M_1}{3s_H v} - \frac{2\sqrt{2}M_2 s_H}{c_H^2 v} - \frac{2\lambda_3 s_H^2}{3c_H^2}. \quad (15)$$

The quartic coupling λ_1 (which depends on λ_5) is computed using

$$\lambda_1 = \frac{1}{8c_H^2 v^2} \left\{ m_h^2 + \frac{3c_H^2 v^2 \left[-M_1 + \sqrt{2}(2\lambda_2 - \lambda_5)s_H v \right]^2}{2\sqrt{2}M_1 \frac{c_H^2}{s_H} v - 6\sqrt{2}M_2 s_H v + 4(\lambda_3 + 3\lambda_4)s_H^2 v^2 - 4m_h^2} \right\}. \quad (16)$$

The mass-squared parameter μ_2^2 (which depends on λ_1 and λ_5) is computed using

$$\mu_2^2 = -4\lambda_1 c_H^2 v^2 - \frac{3}{8}(2\lambda_2 - \lambda_5)s_H^2 v^2 + \frac{3\sqrt{2}}{8}M_1 s_H v, \quad (17)$$

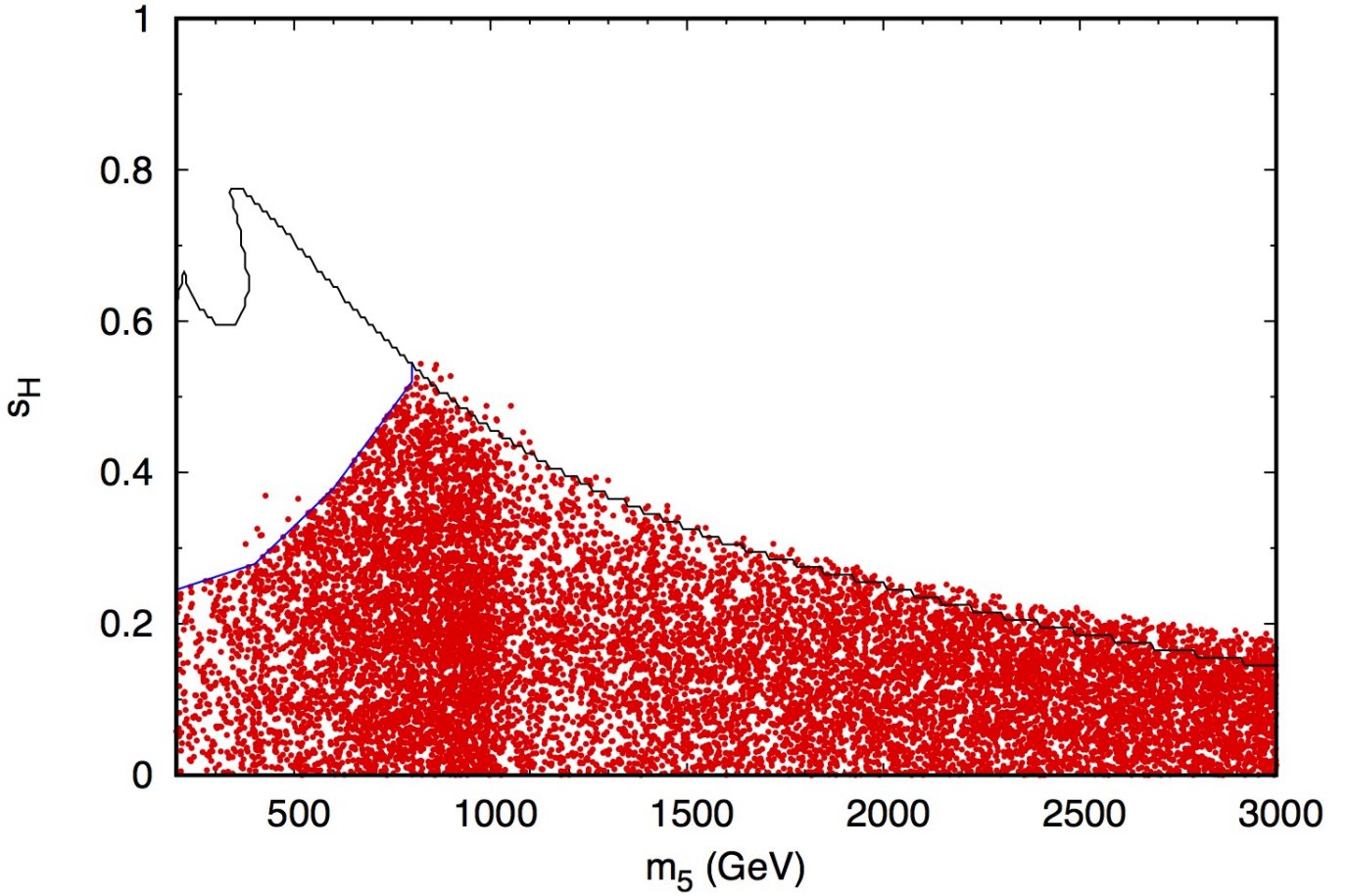


FIG. 1. Theoretically and experimentally allowed parameter region in the m_5 – s_H plane in the H5plane benchmark (entire region below both the black and blue curves) and the full GM model (red points). The black curve delimits the region allowed by theoretical constraints in the H5plane benchmark and the blue curve represents the upper bound on s_H from a direct search for $H_5^{\pm\pm}$ from Ref. [4]. See text for details.

and μ_3^2 is computed using

$$\mu_3^2 = \frac{2}{3}m_5^2 + \frac{\sqrt{2}M_1c_H^2v}{6s_H} - 2\lambda_2c_H^2v^2 - \frac{1}{6}(7\lambda_3 + 9\lambda_4)s_H^2v^2 - \frac{\sqrt{2}}{2}M_2s_Hv. \quad (18)$$

In Fig. 1 we show the allowed region in the m_5 – s_H plane for the full GM model (red points) and the allowed region for the H5plane benchmark scenario (entire region below both the black and blue curves), as generated using GMCALC 1.2.1 with $m_h = 125$ GeV. In both cases we impose the theoretical constraints from perturbative unitarity of the scalar quartic couplings, bounded-from-belowness of the scalar potential, and the absence of deeper alternative minima, as described in Ref. [13], as well as the indirect constraints from $b \rightarrow s\gamma$ and the S parameter following Ref. [15] (we use the “loose” constraint on $b \rightarrow s\gamma$ as described in Ref. [15]); all of these constraints are implemented in GMCALC. We also impose the direct experimental constraint from a CMS search for $H_5^{\pm\pm}$ [4] (described in more detail below), which excludes the area above the blue curve in the context of the H5plane benchmark. The red points represent a scan over the full GM model parameter space. The entire area below the black curve (obtained by scanning m_5 and s_H in the H5plane benchmark) represents the theoretically-allowed region in the H5plane benchmark: as advertised, it nearly, but not quite entirely, populates the entire range of s_H that is accessible in the full GM model for any given value of m_5 between 200 and 3000 GeV. This makes the H5plane scenario a good benchmark for the interpretation of searches for H_5^\pm and $H_5^{\pm\pm}$ in vector boson fusion, for which the signal rate and kinematics depend only on m_5 , s_H , and the H_5 branching ratios into vector boson pairs. We note however that the accessible ranges of other observables are not necessarily fully populated by the H5plane benchmark; this will be particularly dramatic for the mass splittings among the heavy Higgs bosons.

The CMS search in Ref. [4] currently provides the most stringent direct experimental constraint on the GM model

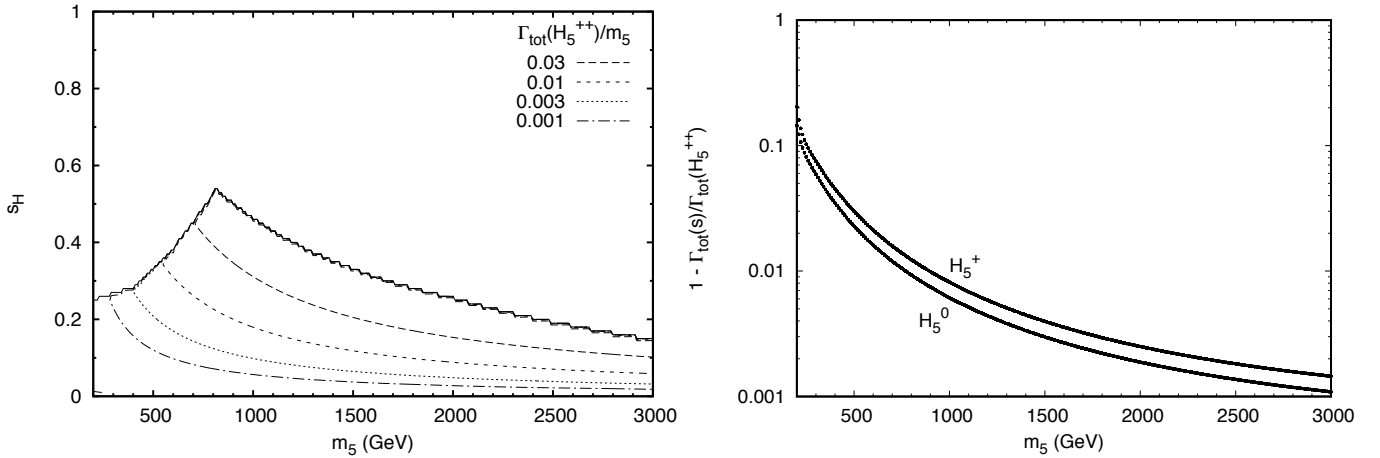


FIG. 2. Left: Contours of Γ_{tot}/m_5 for $H_5^{\pm\pm}$ in the GM model H5plane benchmark. The value of Γ_{tot}/m_5 reaches a maximum of 0.08 along the upper boundary of the allowed region for $m_5 \gtrsim 800$ GeV, and goes to zero at $s_H = 0$. Right: Deviation from unity of the ratio of total widths of scalar $s = H_5^+$ and H_5^0 to that of $H_5^{\pm\pm}$ as a function of m_5 in the H5plane benchmark. Direct constraints from a CMS search for $H_5^{\pm\pm} \rightarrow W^\pm W^\pm$ in vector boson fusion [4] have been applied.

for m_5 above 200 GeV.⁴ This search looked for a doubly-charged scalar produced in vector boson fusion (VBF) and decaying to two like-sign W bosons which in turn decay leptonically, using 19.4 fb^{-1} of proton-proton collision data at a centre-of-mass energy of 8 TeV. This search set a 95% confidence level upper bound on the cross section times branching ratio, $\sigma(\text{VBF} \rightarrow H^{\pm\pm}) \times \text{BR}(H^{\pm\pm} \rightarrow W^\pm W^\pm)$, as a function of the doubly-charged Higgs boson mass. The H5plane benchmark is designed so that $\text{BR}(H_5^{\pm\pm} \rightarrow W^\pm W^\pm) = 1$, so that the CMS constraint becomes an upper bound on the cross section $\sigma(\text{VBF} \rightarrow H_5^{\pm\pm})$, which is proportional to s_H^2 . We translated this into an upper bound on s_H in the H5plane benchmark using the $\text{VBF} \rightarrow H_5^{\pm\pm}$ cross sections calculated for the 8 TeV LHC at next-to-next-to-leading order in QCD in Ref. [10] (we did not take into account the theoretical uncertainties in these predictions in computing the limit). This constraint in the H5plane benchmark is shown as the blue curve in Fig. 1; when combined with the theoretical constraints, it limits $s_H < 0.55$ in the H5plane benchmark. In a full scan of the GM model, some allowed points appear that have $\text{BR}(H_5^{\pm\pm} \rightarrow W^\pm W^\pm) < 1$, because decays into $H_3^\pm W^\pm$ are kinematically allowed. Since the CMS constraint applies to the product $\sigma(\text{VBF} \rightarrow H_5^{\pm\pm}) \times \text{BR}(H_5^{\pm\pm} \rightarrow W^\pm W^\pm)$, this results in a few of the allowed red points in Fig. 1 falling above the blue curve. The number of such points is quite small, though, because most points in the full GM model scan that have $\text{BR}(H_5^{\pm\pm} \rightarrow W^\pm W^\pm) < 1$ also have small s_H , putting them below the blue curve anyway.

III. PROPERTIES OF THE H5PLANE BENCHMARK

A. Decays of H_5

The H5plane benchmark was designed so that $m_3 > m_5$ over the entire benchmark plane, so that the decay $H_5^{\pm\pm} \rightarrow W^\pm W^\pm$ is the only kinematically-allowed decay for $H_5^{\pm\pm}$. This makes direct searches for $H_5^{\pm\pm}$ in the WW final state particularly easy to interpret. Decays of H_5^\pm to $W^\pm Z$ are then also the only kinematically-accessible tree-level decay of H_5^\pm (the loop-induced decay $H_5^\pm \rightarrow W^\pm \gamma$ is allowed, but has a very small branching ratio for $m_5 \geq 200$ GeV), so that direct searches for the singly-charged state in this final state are also easy to interpret. This was used in the GM model interpretation of the ATLAS and CMS searches for H_5^\pm in Refs. [5, 6] (these searches are less constraining on the GM model parameter space than that of Ref. [4]).

In the left panel of Fig. 2 we show the total width of $H_5^{\pm\pm}$ normalized to its mass. This width-to-mass ratio reaches a maximum of 8% for the largest theoretically-allowed values of s_H when $m_5 > 800$ GeV. The right panel of Fig. 2 shows the deviation from unity of the ratio of partial widths of H_5^+ and H_5^0 divided by that of $H_5^{\pm\pm}$ as a function of m_5 . These ratios are independent of s_H . The widths of H_5^+ and H_5^0 are about 10% smaller than that of $H_5^{\pm\pm}$ for

⁴ For comparison, the 95% confidence level constraint obtained in Ref. [8] from an ATLAS measurement of the cross section for like-sign W boson pairs in vector boson fusion [7] excludes s_H values above 0.39 for $m_5 = 200$ GeV, rising to 0.74 for $m_5 = 600$ GeV. LHC searches for H_5^\pm in the WZ final state [5, 6] are currently slightly less constraining than the search for $H_5^{\pm\pm}$.

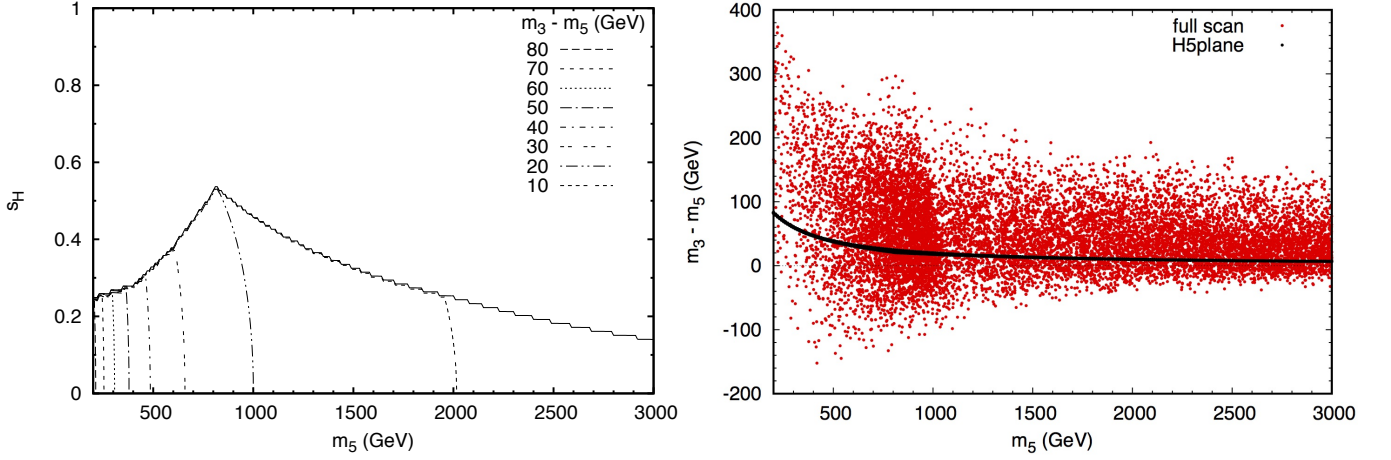


FIG. 3. Left: Contours of $m_3 - m_5$ in the H5plane benchmark. The value of $m_3 - m_5$ ranges from 6.7 GeV to 84 GeV. Right: Mass difference $m_3 - m_5$ as a function of m_5 in the H5plane benchmark (black points) and in a full scan of the GM model parameter space (red points). Indirect constraints from $b \rightarrow s\gamma$ and the S parameter [15] and direct constraints from a CMS search for $H_5^{\pm\pm} \rightarrow W^\pm W^\pm$ in vector boson fusion [4] have been applied.

$m_5 \sim 200$ GeV, with the difference decreasing to less than 1% for $m_5 \gtrsim 1000$ GeV. In the H5plane benchmark, this width difference is solely due to the kinematic effect of the different masses of the WW , WZ , and ZZ final states.

B. H_3 – H_5 mass splitting

In the left panel of Fig. 3 we show the mass splitting $m_3 - m_5$ in the H5plane benchmark. This splitting depends mainly on m_5 , and varies from 84 GeV at $m_5 = 200$ GeV to about 7 GeV at $m_5 = 3000$ GeV. In the right panel of Fig. 3 we plot $m_3 - m_5$ as a function of m_5 scanning over all the other free parameters in the H5plane benchmark (black points) and the full GM model (red points), where we have imposed the indirect constraints from $b \rightarrow s\gamma$ and the S parameter [15] and direct constraints from the CMS search for $H_5^{\pm\pm} \rightarrow W^\pm W^\pm$ in vector boson fusion [4]. It is clear that the variation in the mass difference $m_3 - m_5$ is much greater in the full model scan than it is in the H5plane benchmark. We can understand this as follows.

The difference between m_3^2 and m_5^2 can be written in the full GM model as

$$m_3^2 - m_5^2 = (M_1 - 6M_2) \frac{s_H v}{\sqrt{2}} + \left[\lambda_5 \left(\frac{1}{2} s_H^2 - c_H^2 \right) - \lambda_3 s_H^2 \right] v^2. \quad (19)$$

In the H5plane benchmark, the parameter relations simplify this down to

$$m_3^2 - m_5^2 = (m_3 - m_5)(m_3 + m_5) = \left(\frac{2}{3} - \frac{0.3 s_H^2}{c_H^2} \right) v^2. \quad (20)$$

The variation of this expression with s_H is fairly minimal: $m_3^2 - m_5^2$ changes by less than 10% between $s_H = 0$ and $s_H = 0.4$. This leads to the very narrow range of $m_3 - m_5$ covered by the H5plane benchmark scan (black points) in the right panel of Fig. 3. Solving Eq. (20) for $m_3 - m_5$, the dependence on m_5 is due only to a factor of $1/(m_3 + m_5) \simeq 1/(2m_5)$.

In contrast, in the full GM model scan (red points in the right panel of Fig. 3), $m_3 - m_5$ varies by hundreds of GeV. This is mostly due to the term proportional to $(M_1 - 6M_2)$ in Eq. (19), which is zero in the H5plane benchmark due to the choice $M_2 = M_1/6$, and the term $-\lambda_5 c_H^2 v^2$, which is not suppressed at small s_H . In the full GM model, λ_5 can vary between $-8\pi/3$ and $+8\pi/3$ [13], while in the H5plane benchmark Eq. (15) reduces to

$$\lambda_5 = -\frac{2}{3c_H^2} (1 - 0.1 s_H^2), \quad (21)$$

so that the term $-\lambda_5 c_H^2 v^2$ varies from $2v^2/3$ by less than 2% for s_H between zero and 0.4 in the H5plane benchmark. The preference for positive values of $m_3 - m_5$ in the full GM model scan is due to the interplay of the theoretical

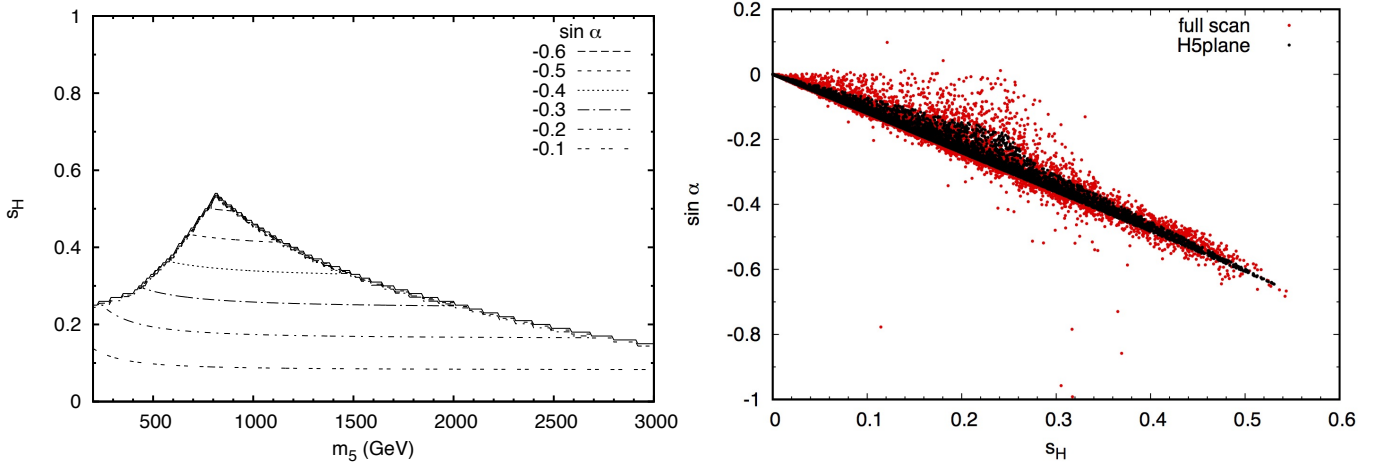


FIG. 4. Left: Contours of $\sin \alpha$ in the H5plane benchmark. The value of $\sin \alpha$ varies between -0.64 and 0 . Right: Correlation between $\sin \alpha$ and s_H in the H5plane benchmark (black points) and in a general GM model scan with $m_5 \geq 200$ GeV (red points). Indirect constraints from $b \rightarrow s\gamma$ and the S parameter [15] and direct constraints from a CMS search for $H_5^{\pm\pm} \rightarrow W^\pm W^\pm$ in vector boson fusion [4] have been applied.

constraints on the model parameters and is apparent already in Fig. 3 of Ref. [15]. Viable mass spectra in the full GM model, and their implications for cascade decays of the heavier Higgs bosons, have previously been studied in Ref. [16].

C. Couplings and decays of h

The tree-level couplings of the 125 GeV Higgs boson h in the GM model are given in terms of the underlying parameters by

$$\kappa_f^h = \frac{c_\alpha}{c_H}, \quad \kappa_V^h = c_\alpha c_H - \sqrt{\frac{8}{3}} s_\alpha s_H, \quad (22)$$

where κ is defined in the usual way as the ratio of the coupling in the GM model to the corresponding coupling of the SM Higgs boson [17].

We first illustrate the variation of the custodial-singlet scalar mixing angle $\sin \alpha$ over the H5plane benchmark in the left panel of Fig. 4. $\sin \alpha$ varies between zero and -0.64 in the H5plane benchmark. It is strongly correlated with s_H , as shown in the right panel of Fig. 4. This correlation also appears in a full scan of the GM model (red points in the right panel of Fig. 4), but is stronger in the H5plane benchmark (black points).

In Fig. 5 we plot κ_f^h (left panel) and κ_V^h (right panel) in the H5plane benchmark. These couplings remain reasonably close to their SM value of 1 everywhere in the benchmark plane. The coupling of h to fermions κ_f^h varies between 0.902 and 1.014, reaching its smallest values when s_H is large, and the coupling of h to vector bosons κ_V^h varies between 1 and 1.21, reaching its largest values when s_H is large.

The coupling of h to photon pairs is affected by the modifications of these tree-level couplings, as well as by contributions from loop diagrams involving H_3^\pm , H_5^\pm , and $H_5^{\pm\pm}$. Defining κ_γ^h in the usual way as [17]⁵

$$\kappa_\gamma^h = \sqrt{\frac{\Gamma(h \rightarrow \gamma\gamma)}{\Gamma(h_{\text{SM}} \rightarrow \gamma\gamma)}}, \quad (23)$$

we plot this coupling in the H5plane benchmark in the left panel of Fig. 6. The coupling of h to photons κ_γ^h varies between 0.99 and 1.24, reaching its largest values when s_H is large. To isolate the effect of the loop diagrams involving

⁵ In GMCALC 1.2.1 the computation of the fermion loop contribution to Higgs decays to two photons includes only the top quark loop.

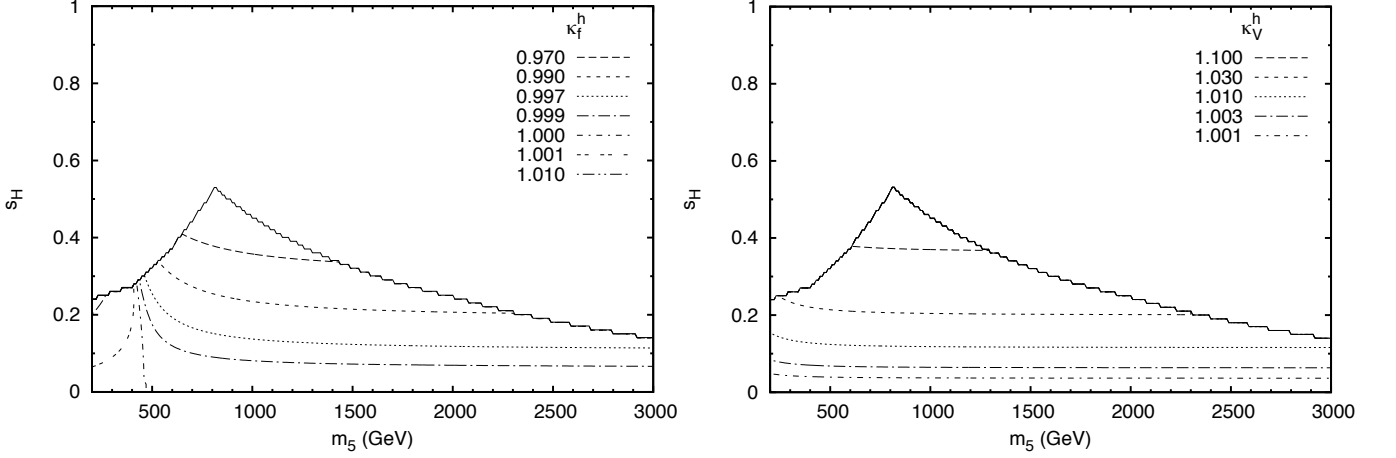


FIG. 5. Left: Contours of κ_f^h in the H5plane benchmark. The value of κ_f^h ranges from 0.902 to 1.014. Right: Contours of κ_V^h in the H5plane benchmark. The value of κ_V^h ranges from 1.00 to 1.21.

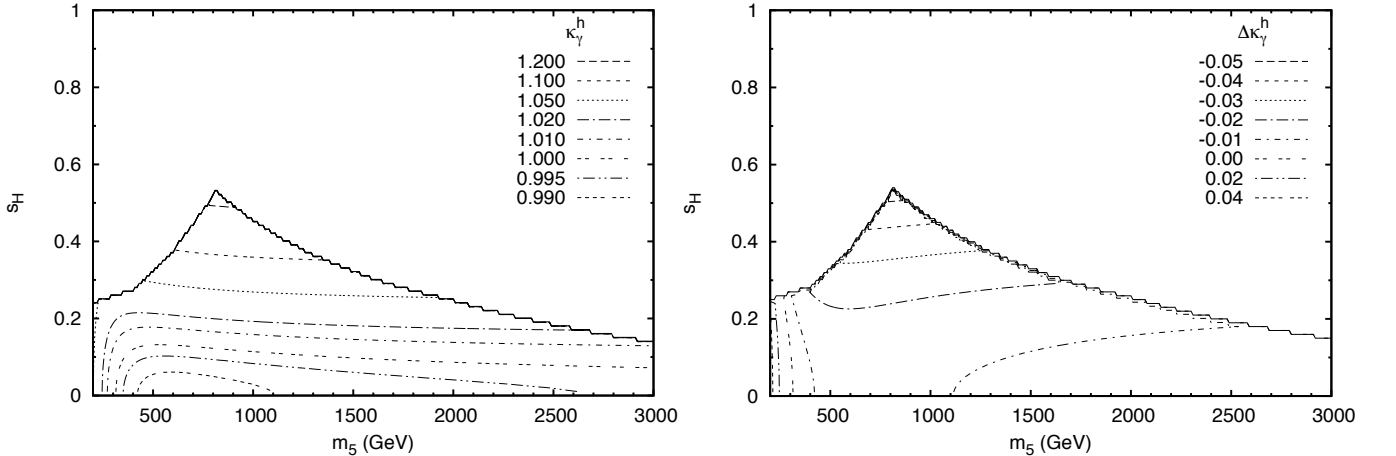


FIG. 6. Left: Contours of κ_γ^h in the H5plane benchmark. The value of κ_γ^h ranges from 0.987 to 1.24. Right: Contours of $\Delta\kappa_\gamma^h$ in the H5plane benchmark. The value of $\Delta\kappa_\gamma^h$ ranges from -0.054 to 0.052 .

H_3^\pm , H_5^\pm , and $H_5^{\pm\pm}$, in the right panel of Fig. 6 we plot $\Delta\kappa_\gamma^h$, which is defined as the contribution to κ_γ^h made by the scalar loops, i.e.,

$$\Delta\kappa_\gamma^h = \kappa_\gamma^h(\text{full}) - \kappa_\gamma^h(\text{t and W loops only}). \quad (24)$$

$\Delta\kappa_\gamma^h$ varies between ± 0.05 in the H5plane benchmark. It is positive only for m_5 below 300 GeV, where it contributes to a slight enhancement of κ_γ^h to values up to 1.05. It reaches its most negative value at large s_H , where it limits the enhancement of κ_γ^h through destructive interference with the dominant W loop contribution.

We also examine the total width of h in the H5plane benchmark. We define the scaling factor κ_h as [17]

$$\kappa_h = \sqrt{\frac{\Gamma_{\text{tot}}(h)}{\Gamma_{\text{tot}}(h_{\text{SM}})}}, \quad (25)$$

and calculate it using the formula

$$\kappa_h^2 = \frac{(\kappa_f^h)^2 \left(B_{h \rightarrow b\bar{b}}^{SM} + B_{h \rightarrow \tau^+\tau^-}^{SM} + B_{h \rightarrow c\bar{c}}^{SM} + B_{h \rightarrow gg}^{SM} \right) + (\kappa_V^h)^2 \left(B_{h \rightarrow W^+W^-}^{SM} + B_{h \rightarrow ZZ}^{SM} \right) + (\kappa_\gamma^h)^2 B_{h \rightarrow \gamma\gamma}^{SM} + (\kappa_{Z\gamma}^h)^2 B_{h \rightarrow \gamma Z}^{SM}}{B_{h \rightarrow b\bar{b}}^{SM} + B_{h \rightarrow \tau^+\tau^-}^{SM} + B_{h \rightarrow c\bar{c}}^{SM} + B_{h \rightarrow gg}^{SM} + B_{h \rightarrow W^+W^-}^{SM} + B_{h \rightarrow ZZ}^{SM} + B_{h \rightarrow \gamma\gamma}^{SM} + B_{h \rightarrow \gamma Z}^{SM}}. \quad (26)$$

branching ratio	value
$B_{h \rightarrow b\bar{b}}^{SM}$	5.809×10^{-1}
$B_{h \rightarrow \tau^+ \tau^-}^{SM}$	6.256×10^{-2}
$B_{h \rightarrow c\bar{c}}^{SM}$	2.884×10^{-2}
$B_{h \rightarrow gg}^{SM}$	8.180×10^{-2}
$B_{h \rightarrow W^+ W^-}^{SM}$	2.152×10^{-1}
$B_{h \rightarrow ZZ}^{SM}$	2.641×10^{-2}
$B_{h \rightarrow \gamma\gamma}^{SM}$	2.270×10^{-3}
$B_{h \rightarrow \gamma Z}^{SM}$	1.541×10^{-3}

TABLE II. Branching ratios of the SM Higgs boson with mass 125.09 GeV, from Ref. [9], used in the calculation of κ_h .

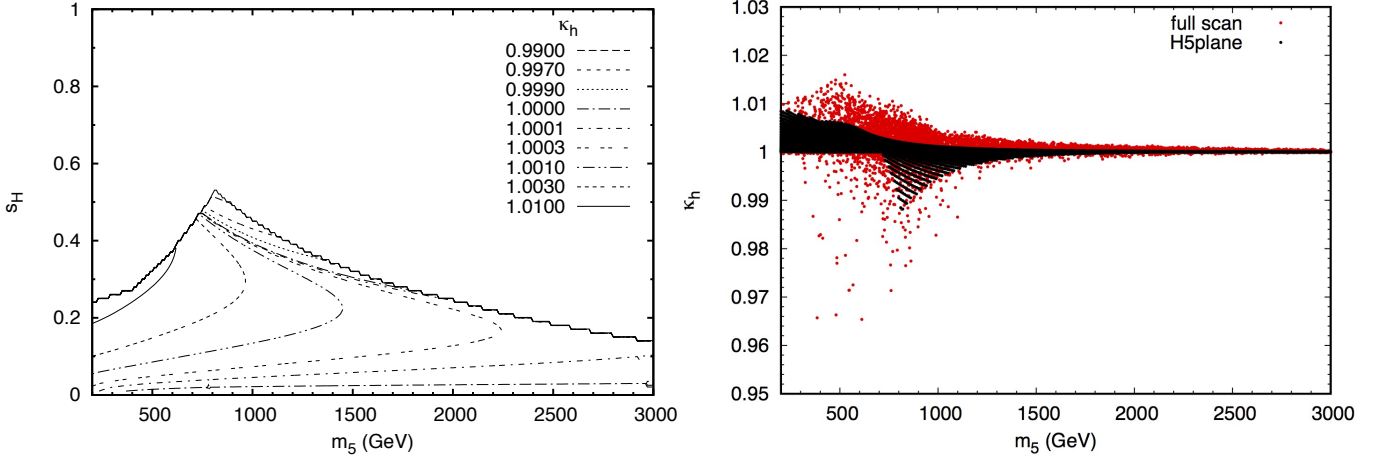


FIG. 7. Left: Contours of κ_h in the H5plane benchmark. The value of κ_h ranges from 0.985 to 1.017. Right: κ_h as a function of m_5 in the H5plane benchmark (black points) and in a full scan of the GM model parameter space (red points). Indirect constraints from $b \rightarrow s\gamma$ and the S parameter [15] and direct constraints from a CMS search for $H_5^{\pm\pm} \rightarrow W^\pm W^\pm$ in vector boson fusion [4] have been applied.

The values for the SM Higgs branching ratios $B_{h \rightarrow X}^{SM}$ were taken from Tables 174–178 of Ref. [9] for a SM Higgs mass of 125.09 GeV and are reproduced in Table II. We use this more precise value of the SM Higgs boson mass in this calculation because the LHC Higgs coupling measurements in Ref. [11] have been extracted for this mass value.

We plot κ_h in the H5plane benchmark in the left panel of Fig. 7. κ_h remains very close to one over the entire benchmark, varying between 0.985 and 1.017, which is surprising considering that the tree-level couplings of h to vector bosons are modified by as much as 21% and those of h to fermions by as much as 10% compared to the SM Higgs couplings. The very SM-like values of the h total width are due to an accidental cancellation between an enhancement of the h partial width to vector bosons and a suppression of its partial width to fermions. This cancellation also occurs, though less severely, in a full scan of the GM model, as shown by the red points in the right panel of Fig. 7. κ_h is slightly greater than one in most of the H5plane benchmark, falling below one in a small sliver at high s_H and m_5 between 700 and 1800 GeV, and in a thin band for $s_H < 0.04$.

In order to evaluate the consistency of the H5plane benchmark with LHC measurements of the couplings of the 125 GeV Higgs boson, we compute a χ^2 using the combined ATLAS and CMS Higgs production and decay measurements in Ref. [11] from data collected at LHC centre-of-mass energies of 7 and 8 TeV. We use the observables and the corresponding correlation matrix ρ summarized in Table 9 and Fig. 28, respectively, of Ref. [11]. The χ^2 is defined according to

$$\chi^2 = (\vec{x} - \vec{\mu})^T V^{-1} (\vec{x} - \vec{\mu}), \quad V_{ij} = \rho_{ij} \sigma_i \sigma_j, \quad (27)$$

where \vec{x} is the vector of observed values, $\vec{\mu}$ is the vector of theoretical values at a particular point in the H5plane benchmark, and $\vec{\sigma}$ is the vector of the combined theoretical and experimental uncertainties. Where the experimental uncertainties in Table 9 of Ref. [11] are asymmetric, we symmetrize them by averaging the upper and lower uncertainty. We then combine the (symmetrized) experimental uncertainties with the theoretical uncertainties quoted in Table 9 of Ref. [11] in quadrature. The results are shown in Fig. 8. The χ^2 in the H5plane benchmark of the GM model ranges

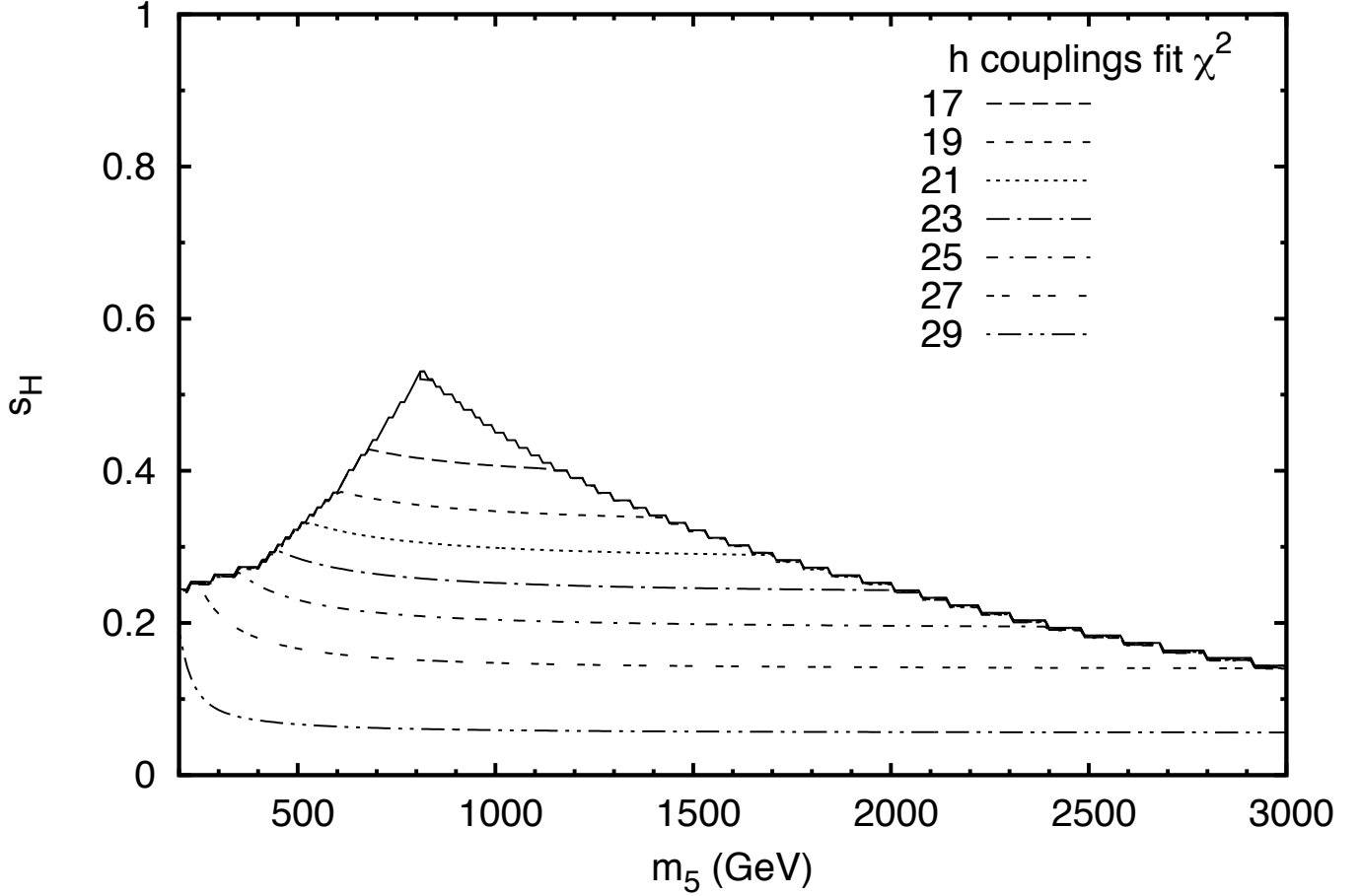


FIG. 8. Contours of the χ^2 value for a fit of the h cross sections and branching ratios in the H5plane benchmark to LHC Higgs boson measurements from Ref. [11]. The χ^2 ranges from 16.2 to 29.9. Compare the χ^2 of 29.4 for the SM Higgs boson.

from a maximum of 29.9 for s_H near zero to a minimum of 16.2 for s_H around 0.5 and m_5 around 800–1000 GeV. For comparison, the χ^2 for the SM Higgs, computed in the same way, is 29.4. The lower χ^2 values in the GM model reflect a pull in the data towards slightly lower κ_f^h and higher κ_V^h values. In particular, we observe that the entire H5plane benchmark is currently consistent with LHC Higgs coupling data.

D. Couplings and decays of H

We now examine the couplings and decays of the heavier custodial-singlet Higgs boson H . The tree-level couplings of H in the GM model are given in terms of the underlying parameters by

$$\kappa_f^H = \frac{s_\alpha}{c_H}, \quad \kappa_V^H = s_\alpha c_H + \sqrt{\frac{8}{3}} c_\alpha s_H, \quad (28)$$

where the κ factors are again defined as the ratio of the H coupling in the GM model to the corresponding coupling of the SM Higgs boson. In Fig. 9 we plot κ_f^H (left panel) and κ_V^H (right panel) in the H5plane benchmark. These couplings are interesting mainly because they control the production of H via gluon fusion and vector boson fusion, respectively. The coupling of H to fermions is largest in magnitude at large s_H , reaching -0.76 times the corresponding SM Higgs coupling. The coupling of H to vector boson pairs is largest at low $m_5 \sim 200$ –300 GeV and large s_H , reaching 0.22 times the corresponding SM Higgs coupling strength. Squaring these, the cross sections for H production by gluon fusion and vector boson fusion reach at most 0.58 and 0.048 times the corresponding SM Higgs cross sections for a Higgs boson of the same mass as H , respectively.

In Figs. 10 and 11 we plot the branching ratios of H to W^+W^- , ZZ , hh , and $t\bar{t}$. These are the dominant decays of H over the entire H5plane benchmark. The branching ratios of H to W^+W^- and ZZ dominate for m_5 below

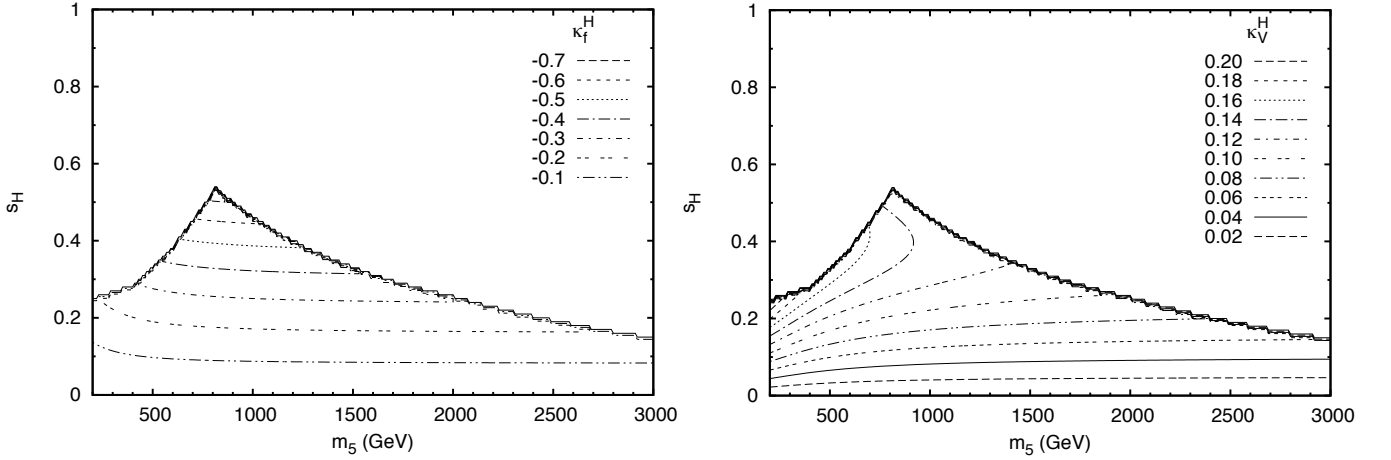


FIG. 9. Contours of κ_f^H (left) and κ_V^H (right) in the H5plane benchmark. κ_f^H ranges from zero to -0.76 and κ_V^H ranges from zero to 0.22 .

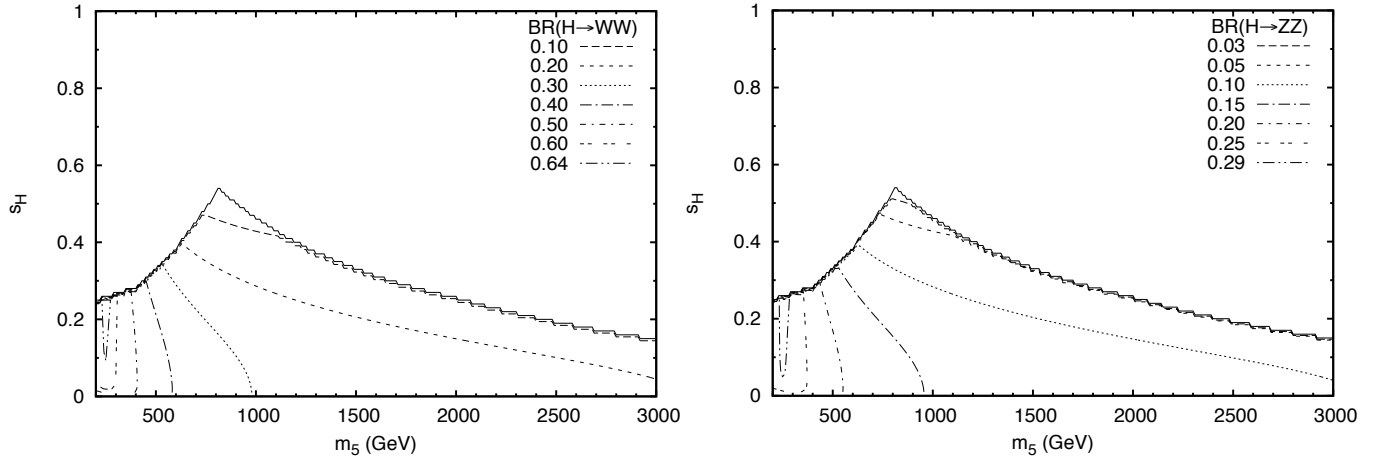


FIG. 10. Contours of $\text{BR}(H \rightarrow W^+W^-)$ (left) and $\text{BR}(H \rightarrow ZZ)$ (right) in the H5plane benchmark. $\text{BR}(H \rightarrow W^+W^-)$ ranges from 0.05 to 0.65 and $\text{BR}(H \rightarrow ZZ)$ ranges from 0.02 to 0.30 .

600 GeV, with branching ratios above 40% and 20%, respectively. These decays reach maximum branching ratios of 65% and 30%, respectively, for low $m_5 \sim 200$ –300 GeV. The branching ratio of H to W^+W^- (ZZ) remains above 20% (10%) over most of the benchmark plane, out to the highest m_5 values.

The branching ratio of H to hh dominates at high masses, reaching 50% for $m_5 \sim 1000$ GeV and a maximum of 71% for the highest s_H values at large $m_5 > 1500$ GeV. The branching ratio of H to $t\bar{t}$ reaches a maximum of 37% for $m_5 \sim 500$ –600 GeV and high s_H , but falls below 10% for $m_5 \gtrsim 1400$ GeV. Note that, because $m_H > m_5$ in the H5plane benchmark, the kinematic threshold for $H \rightarrow t\bar{t}$ at $m_H = 2m_t$ occurs when $m_5 \simeq 250$ GeV.

E. H – H_5 mass splitting

Decays of H_5^+ to HW^+ and of H_5^0 to HZ or HH are forbidden by custodial symmetry. Therefore our interest in the mass splitting between H and H_5^0 is due to the fact that both of these states can be produced in vector boson fusion with decays to W^+W^- and ZZ , which opens the possibility of interference between their lineshapes if the resonances are close enough together. In the left panel of Fig. 12 we show the mass splitting $m_H - m_5$ in the H5plane benchmark. The splitting varies from 120 GeV at $m_5 = 200$ GeV to about 9 GeV at $m_5 = 3000$ GeV. In the right panel of Fig. 12 we plot $m_H - m_5$ as a function of m_5 scanning over all the other free parameters in the H5plane benchmark (black points) and the full GM model (red points), where we have imposed the indirect constraints from $b \rightarrow s\gamma$ and the S parameter [15] and direct constraints from the CMS search for $H_5^{\pm\pm} \rightarrow W^\pm W^\pm$ in vector boson

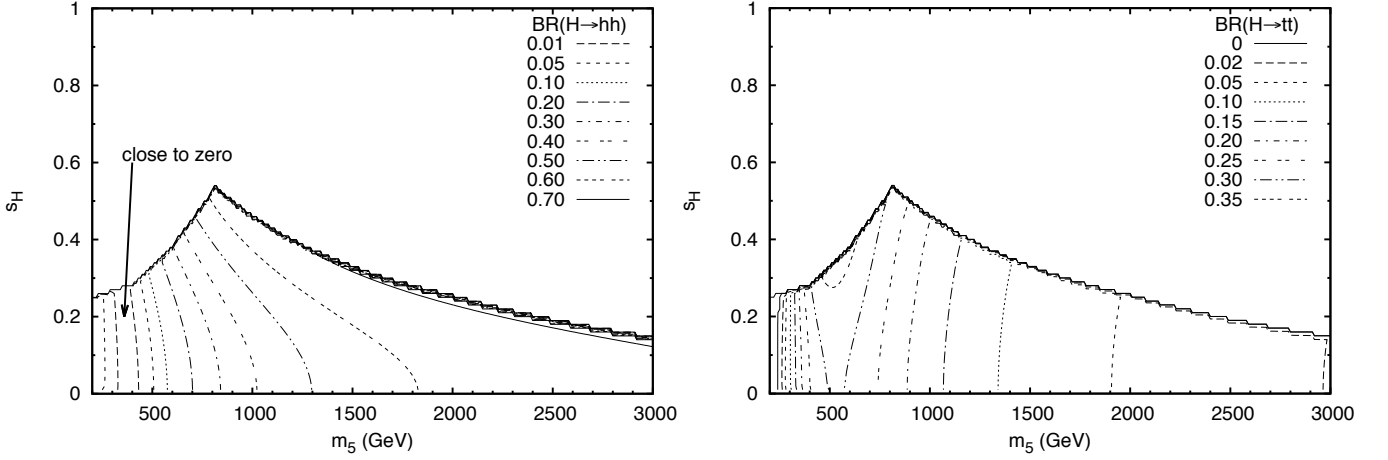


FIG. 11. Contours of $BR(H \rightarrow hh)$ (left) and $BR(H \rightarrow tt)$ (right) in the H5plane benchmark. $BR(H \rightarrow hh)$ ranges from zero to 0.71 and $BR(H \rightarrow tt)$ ranges from zero to 0.37. $BR(H \rightarrow tt)$ drops abruptly to zero when $m_H < 2m_t$ because off-shell decays to $t\bar{t}$ are not calculated in GMCALC 1.2.1.

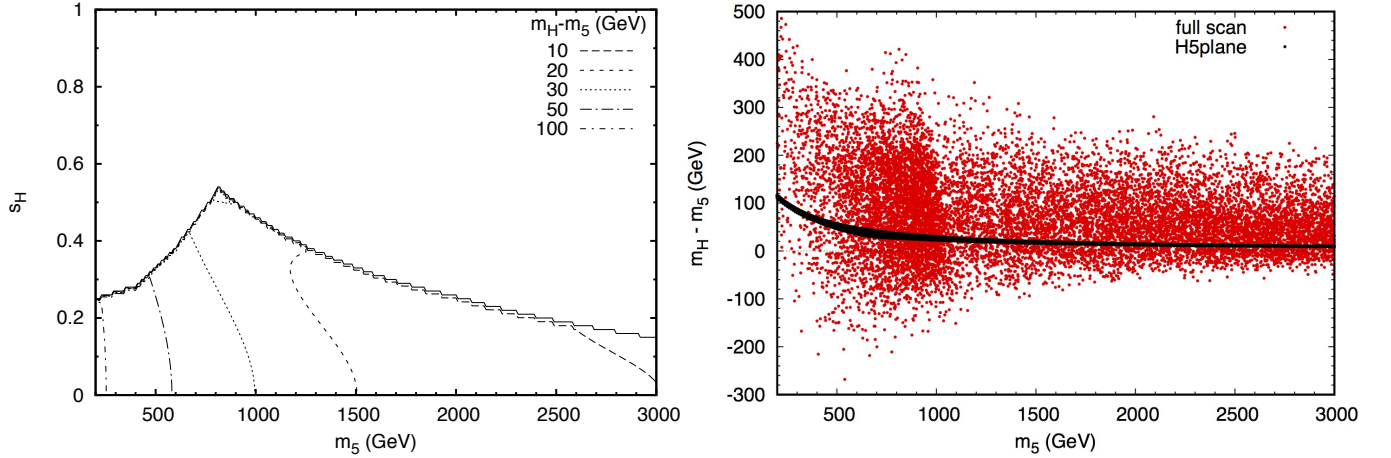


FIG. 12. Left: Contours of $m_H - m_5$ in the H5plane benchmark. $m_H - m_5$ ranges from 8.9 GeV to 120 GeV. Right: Mass difference $m_H - m_5$ as a function of m_5 in the H5plane benchmark (black points) and in a full scan of the GM model parameter space (red points). Indirect constraints from $b \rightarrow s\gamma$ and the S parameter [15] and direct constraints from a CMS search for $H_5^{\pm\pm} \rightarrow W^\pm W^\pm$ in vector boson fusion [4] have been applied.

fusion [4]. Similarly to the case of $m_3 - m_5$, we see that the variation in the mass difference $m_H - m_5$ is much greater in the full model scan than it is in the H5plane benchmark.

To understand the experimental implications of this mass splitting, we compare it to the intrinsic widths of H and H_5^0 . In Fig. 13 we first plot the total width of H (top left panel) and the ratio $\Gamma_{\text{tot}}(H)/\Gamma_{\text{tot}}(H_5^0)$ (top right panel) in the H5plane benchmark. The total widths of H and H_5^0 are very similar for $m_5 \gtrsim 500$ GeV. For lower masses, the fact that H is significantly heavier than H_5^0 allows its width to become more than twice as large as that of H_5^0 for $m_5 < 450$ GeV. Over the entire H5plane benchmark, the width of H is never less than 89% of the width of H_5^0 .

Therefore we can quantify the $H - H_5^0$ mass splitting by comparing it to the total width of H . We do this in the bottom panel of Fig. 13, in which we plot $(m_H - m_5)/\Gamma_{\text{tot}}(H)$ over the H5plane benchmark. This ratio varies widely over the benchmark. For low m_5 and low s_H , $(m_H - m_5)/\Gamma_{\text{tot}}(H)$ is large, which means that the H and H_5^0 resonances are well separated compared to their intrinsic widths. However, there is a sizable region of parameter space in which $(m_H - m_5)/\Gamma_{\text{tot}}(H) < 1$, which means that the mass splitting is less than the intrinsic width of H . In this region of the H5plane benchmark, the total width of H_5^0 is within 10% of that of H . In this case the two resonances overlap significantly and interfere, so that experimental searches for these two states in vector boson fusion with decays to W^+W^- or ZZ must be performed taking into account both resonances and their interference. Interference can be avoided by searching for H produced in gluon fusion, or decaying to hh or $t\bar{t}$.

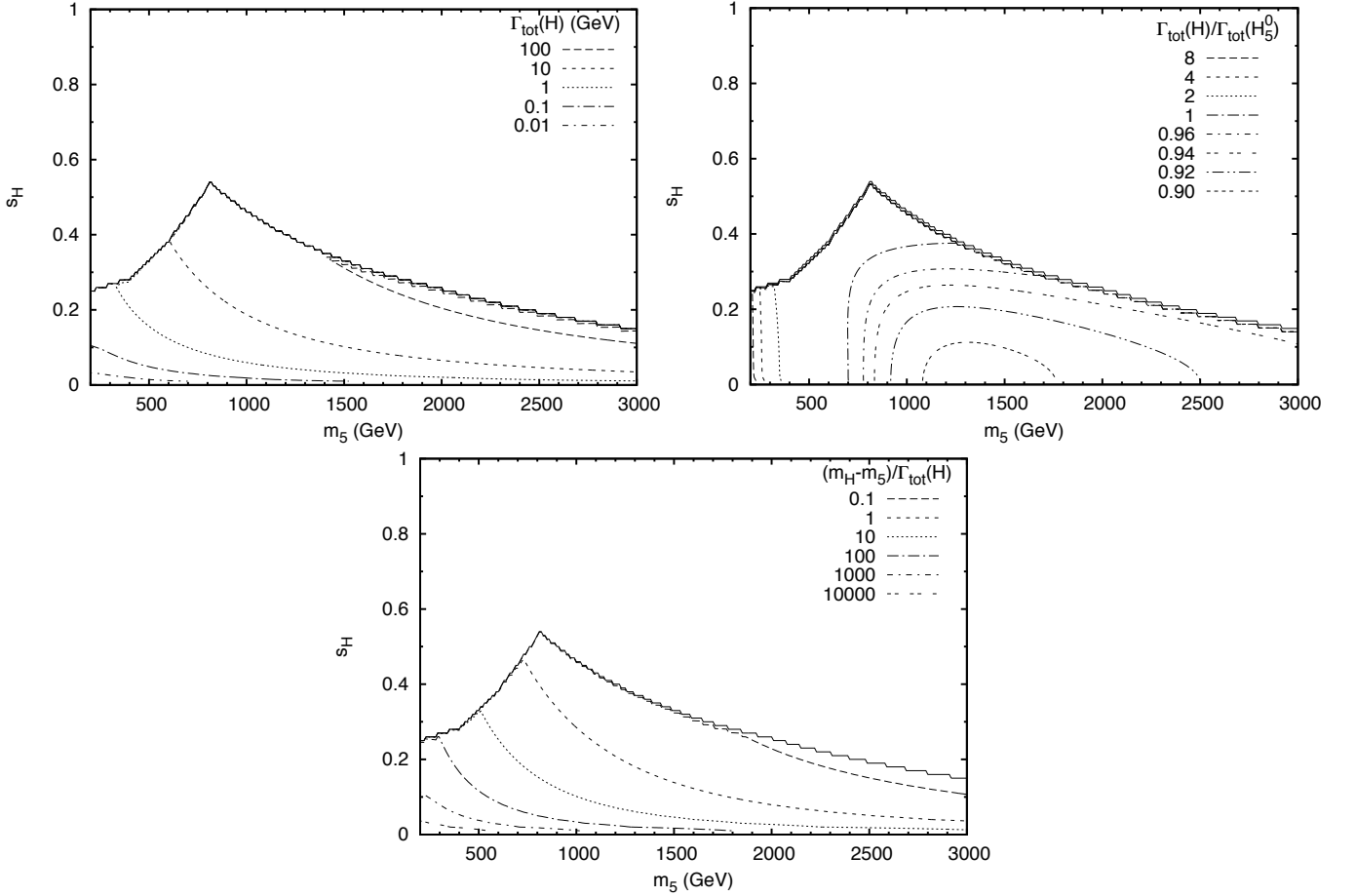


FIG. 13. Top left: Contours of the total width of H , $\Gamma_{\text{tot}}(H)$, in the H5plane benchmark. $\Gamma_{\text{tot}}(H)$ ranges from 0.0013 GeV to 170 GeV. Top right: Contours of the ratio $\Gamma_{\text{tot}}(H)/\Gamma_{\text{tot}}(H_5^0)$ in the H5plane benchmark. $\Gamma_{\text{tot}}(H)/\Gamma_{\text{tot}}(H_5^0)$ ranges from 0.89 to 16. Bottom: Contours of $(m_H - m_5)/\Gamma_{\text{tot}}(H)$ in the H5plane benchmark. $(m_H - m_5)/\Gamma_{\text{tot}}(H)$ ranges from 0.054 to 89000.

F. Decays of H_3

The dominant decays of H_3^0 in the H5plane benchmark are to $t\bar{t}$, hZ , H_5^0Z , and $H_5^{\pm}W^{\mp}$. (H_3^0 can also decay to two photons; however, $\text{BR}(H_3^0 \rightarrow \gamma\gamma)$ stays below 1.8×10^{-4} over the entire H5plane benchmark.) We plot the branching ratios for these modes in Figs. 14 and 15. The kinematic threshold for $H_3^0 \rightarrow t\bar{t}$ at $m_3 = 2m_t$ occurs at m_5 just below 300 GeV. Once above this threshold, $\text{BR}(H_3^0 \rightarrow t\bar{t})$ quickly rises to a maximum of 79% for $m_5 \sim 300\text{--}400$ GeV, and then falls with increasing m_5 . The next-largest fermionic decay branching ratio of H_3^0 is to $b\bar{b}$, which is below 1% over almost all of the H5plane benchmark. The branching ratio of H_3^0 to hZ exhibits complementary behaviour, growing with m_5 to become the dominant decay mode (> 50%) for $m_5 \gtrsim 500$ GeV and surpassing 90% branching ratio for $m_5 \gtrsim 1200$ GeV.

The branching ratios of H_3^0 to H_5^0Z and $H_5^{\pm}W^{\mp}$ (we plot the sum of the branching ratios to $H_5^+W^-$ and $H_5^-W^+$) are significant only for very low m_5 , below the kinematic threshold for the $t\bar{t}$ decay. For these low masses, the branching ratios of these modes can be quite large, reaching respective values of 85% and 82% in our calculation, in slightly different areas of parameter space. However, these numbers should be treated with caution because the implementation in GMCALC 1.2.1 of scalar decays to scalar plus vector at and below the kinematic threshold is still rather primitive. At $m_5 = 200$ GeV, the mass splitting between H_3 and H_5 in the H5plane benchmark is 84 GeV, so that the on-shell decay $H_3^0 \rightarrow H_5^{\pm}W^{\mp}$ is barely kinematically allowed, while $H_3^0 \rightarrow H_5^0Z$ is off shell. As m_5 increases, the mass splitting decreases, and $H_3^0 \rightarrow H_5^{\pm}W^{\mp}$ goes off shell at $m_5 \simeq 210$ GeV. Above threshold, GMCALC 1.2.1 computes these decay widths using the two-body on-shell decay formula, while below threshold the computation takes into account the offshellness of the vector boson only. This is a reasonable approximation at $m_5 \sim 200$ GeV where the H_5 scalars are very narrow; however, the transition from the on-shell to off-shell decay widths is not smooth. The handling of this transition, along with off-shell decays of $H_3^0 \rightarrow t\bar{t}$, should be improved if detailed predictions for the

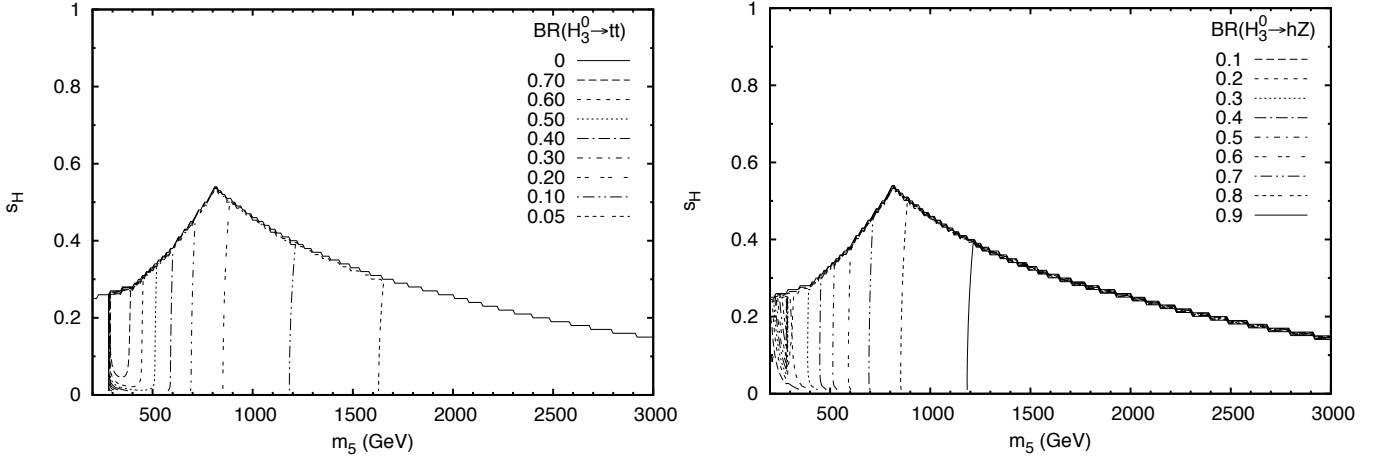


FIG. 14. Left: Contours of $\text{BR}(H_3^0 \rightarrow t\bar{t})$ in the H5plane benchmark. $\text{BR}(H_3^0 \rightarrow t\bar{t})$ ranges from zero to 0.79. Below the kinematic threshold at $m_3 = 2m_t$, the branching ratio drops to zero because off-shell decays to $t\bar{t}$ are not calculated in **GMCALC 1.2.1**. $\text{BR}(H_3^0 \rightarrow t\bar{t})$ reaches a maximum of 0.79 and falls to 0.013 at $m_5 = 3000$ GeV. Right: Contours of $\text{BR}(H_3^0 \rightarrow hZ)$ in the H5plane benchmark. $\text{BR}(H_3^0 \rightarrow hZ)$ ranges from 2×10^{-4} to 0.987. In the band $m_5 \in (200 \text{ GeV}, 300 \text{ GeV})$, the branching ratio increases rapidly, up to nearly 0.9 for $m_5 = 280$ GeV, before collapsing down to about 0.2; $\text{BR}(H_3^0 \rightarrow hZ)$ then rises with increasing m_5 . The sudden drop in $\text{BR}(H_3^0 \rightarrow hZ)$ is due to crossing the kinematic threshold for $H_3^0 \rightarrow t\bar{t}$.

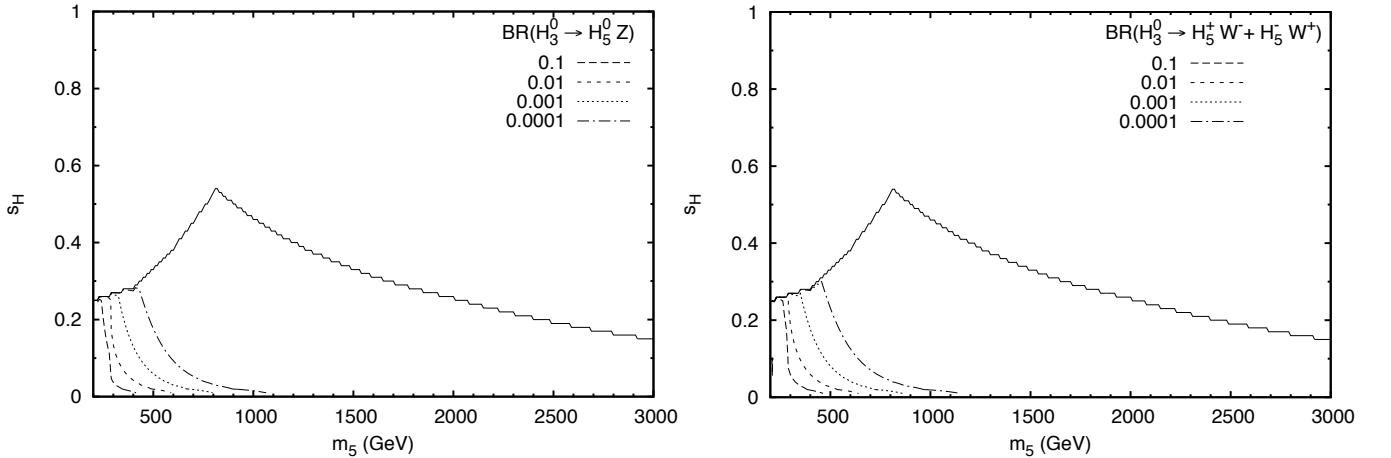


FIG. 15. Contours of $\text{BR}(H_3^0 \rightarrow H_5^0 Z)$ (left) and $\text{BR}(H_3^0 \rightarrow H_5^{\pm} W^{\mp} + H_5^{\mp} W^{\pm})$ (right) in the H5plane benchmark. See text for further discussion.

H_3^0 branching ratios for $m_5 \lesssim 280$ GeV are needed. The branching ratios for H_3^0 to $H_5^0 Z$ and $H_5^{\pm} W^{\mp}$ fall below 1% for $m_5 \gtrsim 500$ GeV.

The dominant decays of H_3^+ in the H5plane benchmark are to $t\bar{b}$, hW^+ , $H_5^0 W^+$, $H_5^+ Z$, and $H_5^{++} W^-$. We plot the branching ratios for these modes in Figs. 16 and 17. The decay to $t\bar{b}$ dominates at low m_5 , reaching a maximum of more than 95% for $m_5 \sim 250$ GeV. This branching ratio falls with increasing m_5 and is supplanted by the decay to hW^+ . The branching ratio for $H_3^+ \rightarrow hW^+$ becomes dominant ($> 50\%$) for $m_5 \gtrsim 500$ GeV and surpasses 90% when $m_5 \gtrsim 1200$ GeV.

The branching ratios of H_3^+ to $H_5^0 W^+$, $H_5^+ Z$, and $H_5^{++} W^-$ are significant only for very low values of both m_5 and s_H within the H5plane benchmark. In this corner of parameter space, the branching ratios of these modes can be significant, reaching maxima of 25%, 79%, and 49%, respectively, in slightly different regions of parameter space. Again, though, these numbers should be treated with caution because the decays of H_3^+ to $H_5 V$ face the same issues with the transition from on shell to off shell as the decays of H_3^0 to $H_5 V$. All three of these branching ratios quickly fall below the 1% level for $m_5 \gtrsim 500$ GeV. These decay modes also decline quickly with increasing s_H , due to an increase in the partial width for $H_3^+ \rightarrow t\bar{b}$ with increasing s_H .

Finally, we plot the total widths of H_3^0 and H_3^+ in Fig. 18. They both remain quite small over the entire allowable region: although they do increase with increasing s_H and m_5 , the width-to-mass ratio $\Gamma_{\text{tot}}(H_3)/m_3$ never rises above

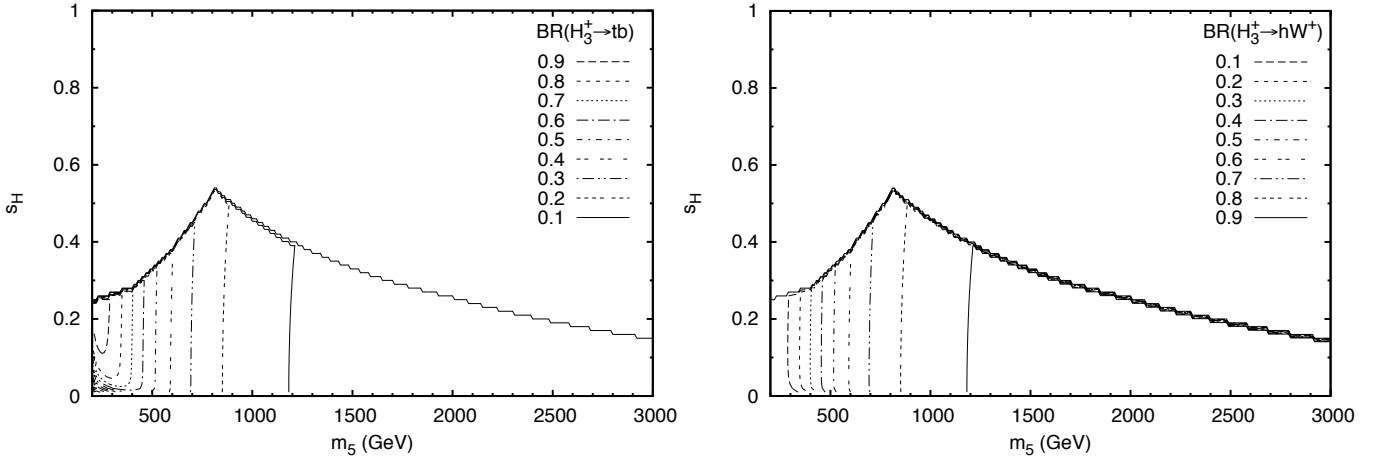


FIG. 16. Contours of $BR(H_3^+ \rightarrow t\bar{b})$ (left) and $BR(H_3^+ \rightarrow hW^+)$ (right) in the H5plane benchmark. $BR(H_3^+ \rightarrow t\bar{b})$ ranges from 0.013 to 0.964 and $BR(H_3^+ \rightarrow hW^+)$ ranges from 3×10^{-4} to 0.987.

8% for either H_3^0 or H_3^+ .

IV. CONCLUSIONS

In this paper we studied the constraints on and phenomenology of the H5plane benchmark scenario in the Georgi-Machacek model. The H5plane benchmark has two free parameters, m_5 and s_H , where s_H^2 is equal to the fraction of M_W^2 and M_Z^2 that is generated by the vev of the isospin triplets. The H5plane benchmark is defined for $m_5 \in [200, 3000]$ GeV. Existing theoretical and experimental constraints limit s_H to be below 0.55 in the H5plane benchmark, so that at most 30% of the W and Z boson squared-masses can be generated by the triplets. A full parameter scan of the GM model yields an allowed region in the m_5 – s_H plane only slightly larger than in the H5plane benchmark for $m_5 \in [200, 3000]$ GeV. Our numerical work has been done using the public code **GMCALC 1.2.1**.

We showed that the couplings of the 125 GeV Higgs boson h in the H5plane benchmark are sufficiently SM-like that the benchmark is not further constrained by the ATLAS and CMS measurements of Higgs production and decay at LHC center-of-mass energies of 7 and 8 TeV—in fact, over most of the H5plane benchmark, the fit to LHC data is slightly better than in the SM. Over the H5plane benchmark, compared to their SM values, the h coupling to fermions can be suppressed by up to 10% or enhanced by up to 1.4%, its coupling to vector boson pairs can be enhanced by up to 21%, and its loop-induced coupling to photon pairs can be suppressed by up to 1.3% or enhanced by up to 24% (loops involving the charged scalars in the GM model contribute non-negligibly to this). The total width of h can be suppressed by up to 2.9% or enhanced by up to 3.5% compared to that of the SM Higgs boson; the smallness of this range is due to an accidental cancellation among the fermionic and bosonic contributions.

By design, the mass-degenerate $H_5^{\pm\pm}$, H_5^{\pm} , and H_5^0 scalars are the lightest new scalars in the H5plane benchmark, and hence decay only to vector boson pairs at tree level. Due to the parameter specifications in the benchmark, the mass splittings $m_3 - m_5$ and $m_H - m_5$ are almost constant with s_H , depending primarily on m_5 . They fall from maxima of 84 and 120 GeV, respectively, at $m_5 = 200$ GeV to minima of 7 and 9 GeV, respectively, at $m_5 = 3000$ GeV. (These mass splittings vary much more freely in the full GM model.) While the mass-to-width ratios of all the new scalars in the GM model remain below 8% in the H5plane benchmark, the fairly small mass splitting between H_5^0 and H means that these two resonances can overlap and interfere when produced in vector boson fusion and decaying to W^+W^- or ZZ . Their mass splitting becomes smaller than their intrinsic widths when $m_5 \gtrsim 700$ GeV, unless s_H is small.

Finally we studied the production and decays of the new heavy Higgs bosons in the GM model in the H5plane benchmark. We found that, due to coupling suppressions, the production cross section of H in gluon fusion (vector boson fusion) can be at most 58% (4.8%) as large as that of a SM Higgs boson of the same mass. H decays mainly to W^+W^- and ZZ for m_5 below 600–1000 GeV (depending on s_H), and mainly to hh for m_5 above 700–1300 GeV. Its branching ratio to $t\bar{t}$ can top 30% for m_5 between 400 and 700 GeV.

H_3^0 decays predominantly to $t\bar{t}$ from the kinematic threshold at $m_5 = 280$ GeV up to $m_5 \simeq 500$ GeV, where hZ takes over as the dominant decay mode. Below the $t\bar{t}$ threshold, decays to H_5^0Z and $H_5^{\pm}W^{\mp}$ can be significant, but improvements to the handling of near-threshold decays in **GMCALC** are needed to fully explore the branching ratios

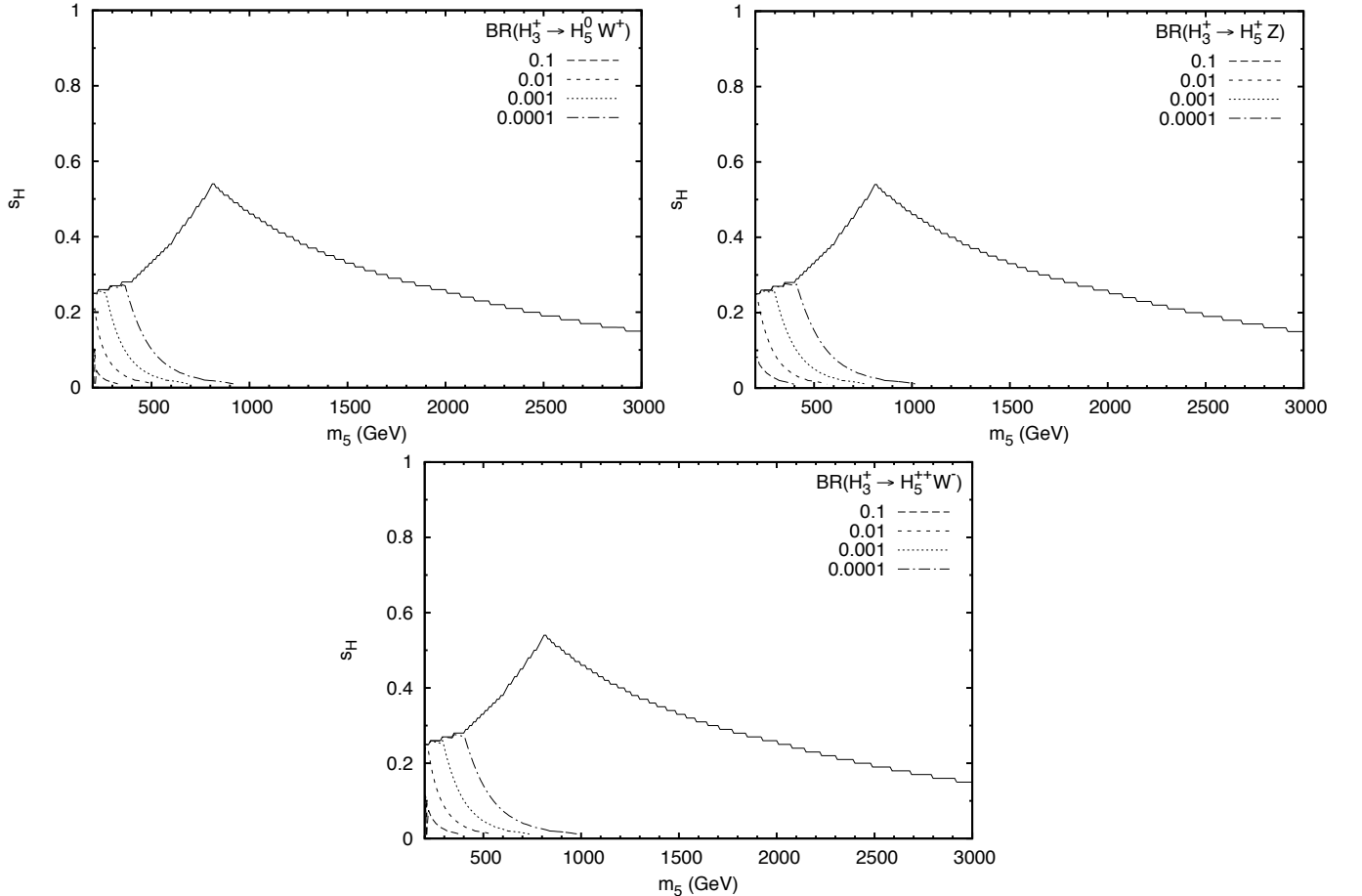


FIG. 17. Contours of $\text{BR}(H_3^+ \rightarrow H_5^0 W^+)$ (top left), $\text{BR}(H_3^+ \rightarrow H_5^+ Z)$ (top right), and $\text{BR}(H_3^+ \rightarrow H_5^{++} W^-)$ (bottom) in the H_5 plane benchmark. See text for further discussion.

in this region. H_3^+ decays predominantly to $t\bar{b}$ for m_5 values up to about 500 GeV, where hW^+ takes over as the dominant decay mode.

ACKNOWLEDGMENTS

We thank Dag Gillberg for helpful conversations. This work was supported by the Natural Sciences and Engineering Research Council of Canada. H.E.L. was also partially supported through the grant H2020-MSCA-RISE-2014 no. 645722 (NonMinimalHiggs).

[1] G. Aad *et al.* [ATLAS Collaboration], “Observation of a new particle in the search for the Standard Model Higgs boson with the ATLAS detector at the LHC,” *Phys. Lett. B* **716**, 1 (2012) [arXiv:1207.7214 [hep-ex]]; S. Chatrchyan *et al.* [CMS Collaboration], “Observation of a new boson at a mass of 125 GeV with the CMS experiment at the LHC,” *Phys. Lett. B* **716**, 30 (2012) [arXiv:1207.7235 [hep-ex]].

[2] H. Georgi and M. Machacek, “Doubly Charged Higgs Bosons,” *Nucl. Phys. B* **262**, 463 (1985).

[3] M. S. Chanowitz and M. Golden, “Higgs Boson Triplets With $M(W) = M(Z) \cos \theta_W$,” *Phys. Lett.* **165B**, 105 (1985).

[4] V. Khachatryan *et al.* [CMS Collaboration], “Study of vector boson scattering and search for new physics in events with two same-sign leptons and two jets,” *Phys. Rev. Lett.* **114**, no. 5, 051801 (2015) [arXiv:1410.6315 [hep-ex]].

[5] G. Aad *et al.* [ATLAS Collaboration], “Search for a Charged Higgs Boson Produced in the Vector-Boson Fusion Mode with Decay $H^\pm \rightarrow W^\pm Z$ using pp Collisions at $\sqrt{s} = 8$ TeV with the ATLAS Experiment,” *Phys. Rev. Lett.* **114**, no. 23, 231801 (2015) [arXiv:1503.04233 [hep-ex]].

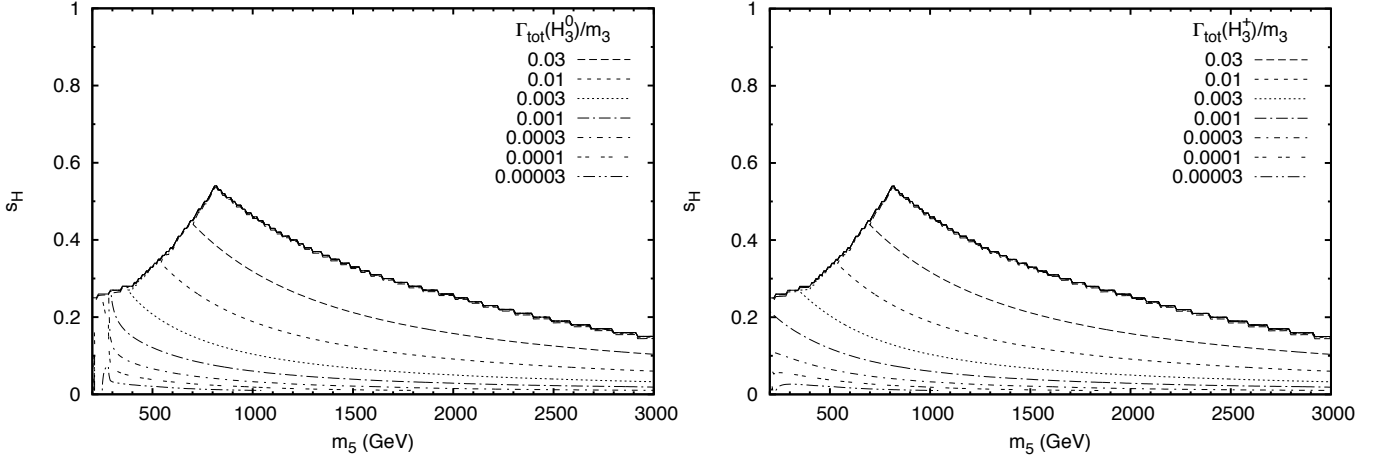


FIG. 18. Contours of $\Gamma_{\text{tot}}(H_3^0)/m_3$ (left) and $\Gamma_{\text{tot}}(H_3^+)/m_3$ (right) in the H5 plane benchmark. $\Gamma_{\text{tot}}(H_3^0)/m_3$ ranges from 6.6×10^{-6} to 0.077 and $\Gamma_{\text{tot}}(H_3^+)/m_3$ ranges from 6.2×10^{-6} to 0.077.

- [6] A. M. Sirunyan *et al.* [CMS Collaboration], “Search for charged Higgs bosons produced in vector boson fusion processes and decaying into a pair of W and Z bosons using proton-proton collisions at $\sqrt{s} = 13$ TeV,” arXiv:1705.02942 [hep-ex].
- [7] G. Aad *et al.* [ATLAS Collaboration], “Evidence for Electroweak Production of $W^\pm W^\pm jj$ in pp Collisions at $\sqrt{s} = 8$ TeV with the ATLAS Detector,” Phys. Rev. Lett. **113**, no. 14, 141803 (2014) [arXiv:1405.6241 [hep-ex]].
- [8] C. W. Chiang, S. Kanemura and K. Yagyu, “Novel constraint on the parameter space of the Georgi-Machacek model with current LHC data,” Phys. Rev. D **90**, no. 11, 115025 (2014) [arXiv:1407.5053 [hep-ph]].
- [9] D. de Florian *et al.* [LHC Higgs Cross Section Working Group], “Handbook of LHC Higgs Cross Sections: 4. Deciphering the Nature of the Higgs Sector,” arXiv:1610.07922 [hep-ph].
- [10] M. Zaro and H. Logan, “Recommendations for the interpretation of LHC searches for H_5^0 , H_5^\pm , and $H_5^{\pm\pm}$ in vector boson fusion with decays to vector boson pairs,” LHC HXSWG-2015-001, available from <https://cds.cern.ch/record/2002500>.
- [11] G. Aad *et al.* [ATLAS and CMS Collaborations], “Measurements of the Higgs boson production and decay rates and constraints on its couplings from a combined ATLAS and CMS analysis of the LHC pp collision data at $\sqrt{s} = 7$ and 8 TeV,” JHEP **1608**, 045 (2016) [arXiv:1606.02266 [hep-ex]].
- [12] K. Hartling, K. Kumar and H. E. Logan, “GMCALC: a calculator for the Georgi-Machacek model,” arXiv:1412.7387 [hep-ph].
- [13] K. Hartling, K. Kumar and H. E. Logan, “The decoupling limit in the Georgi-Machacek model,” Phys. Rev. D **90**, no. 1, 015007 (2014) [arXiv:1404.2640 [hep-ph]].
- [14] M. Aoki and S. Kanemura, “Unitarity bounds in the Higgs model including triplet fields with custodial symmetry,” Phys. Rev. D **77**, no. 9, 095009 (2008) [Erratum: Phys. Rev. D **89**, no. 5, 059902 (2014)] [arXiv:0712.4053 [hep-ph]].
- [15] K. Hartling, K. Kumar and H. E. Logan, “Indirect constraints on the Georgi-Machacek model and implications for Higgs boson couplings,” Phys. Rev. D **91**, no. 1, 015013 (2015) [arXiv:1410.5538 [hep-ph]].
- [16] C. W. Chiang, A. L. Kuo and T. Yamada, “Searches of exotic Higgs bosons in general mass spectra of the Georgi-Machacek model at the LHC,” JHEP **1601**, 120 (2016) [arXiv:1511.00865 [hep-ph]].
- [17] A. David *et al.* [LHC Higgs Cross Section Working Group], “LHC HXSWG interim recommendations to explore the coupling structure of a Higgs-like particle,” arXiv:1209.0040 [hep-ph].